

Supporting Information

Thermodynamically Consistent Force Fields for the Assembly of Inorganic, Organic, and
Biological Nanostructures: The INTERFACE Force Field

By

Hendrik Heinz, Tzu-Jen Lin, Ratan Kishore Mishra, Fateme Sadat Emami

Department of Polymer Engineering, University of Akron, Akron, OH 44325

Email: hendrik.heinz@uakron.edu

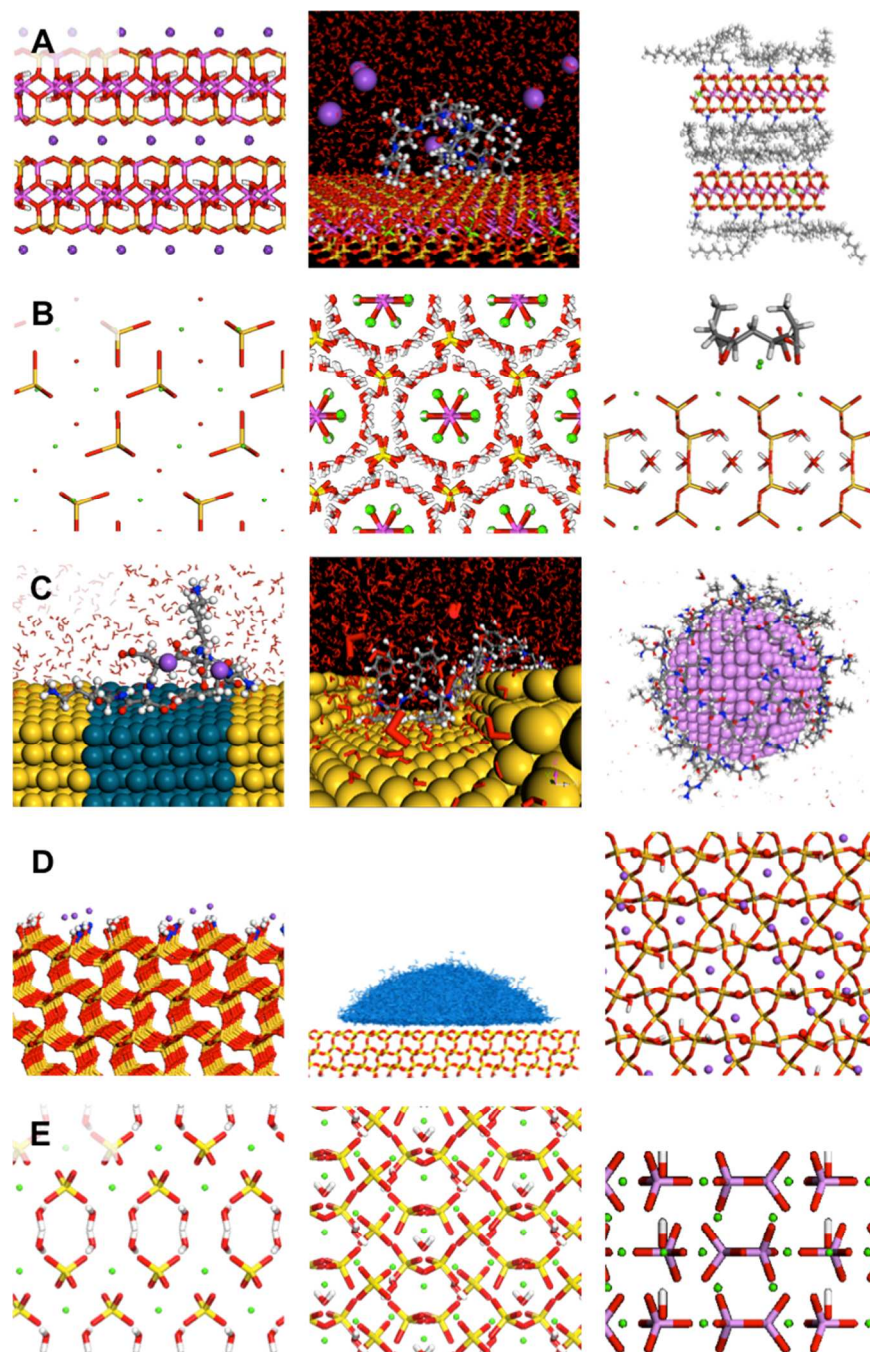


Figure S1. Examples of structures and interfaces simulated using the INTERFACE force field (left to right in each row). (A) Layered silicates, including mica, montmorillonite in contact with a peptide in aqueous solution, and montmorillonite modified with alkylammonium surfactants. (B) Cement minerals, depicting tricalcium silicate, ettringite, and tobermorite 11 Å in contact with an organic additive. (C) Fcc metals with the examples of a gold-palladium bimetal surface, a stepped gold surface, and a platinum nanoparticle in contact with peptides in aqueous solution. (D) An ionized Q^3 silica surface, water in contact with a Q^4 silica surface, and top view onto an ionized Q^2 silica surface. (E) Impressions of the crystal structures of gypsum, calcium sulphate hemihydrate, and hydroxyapatite.

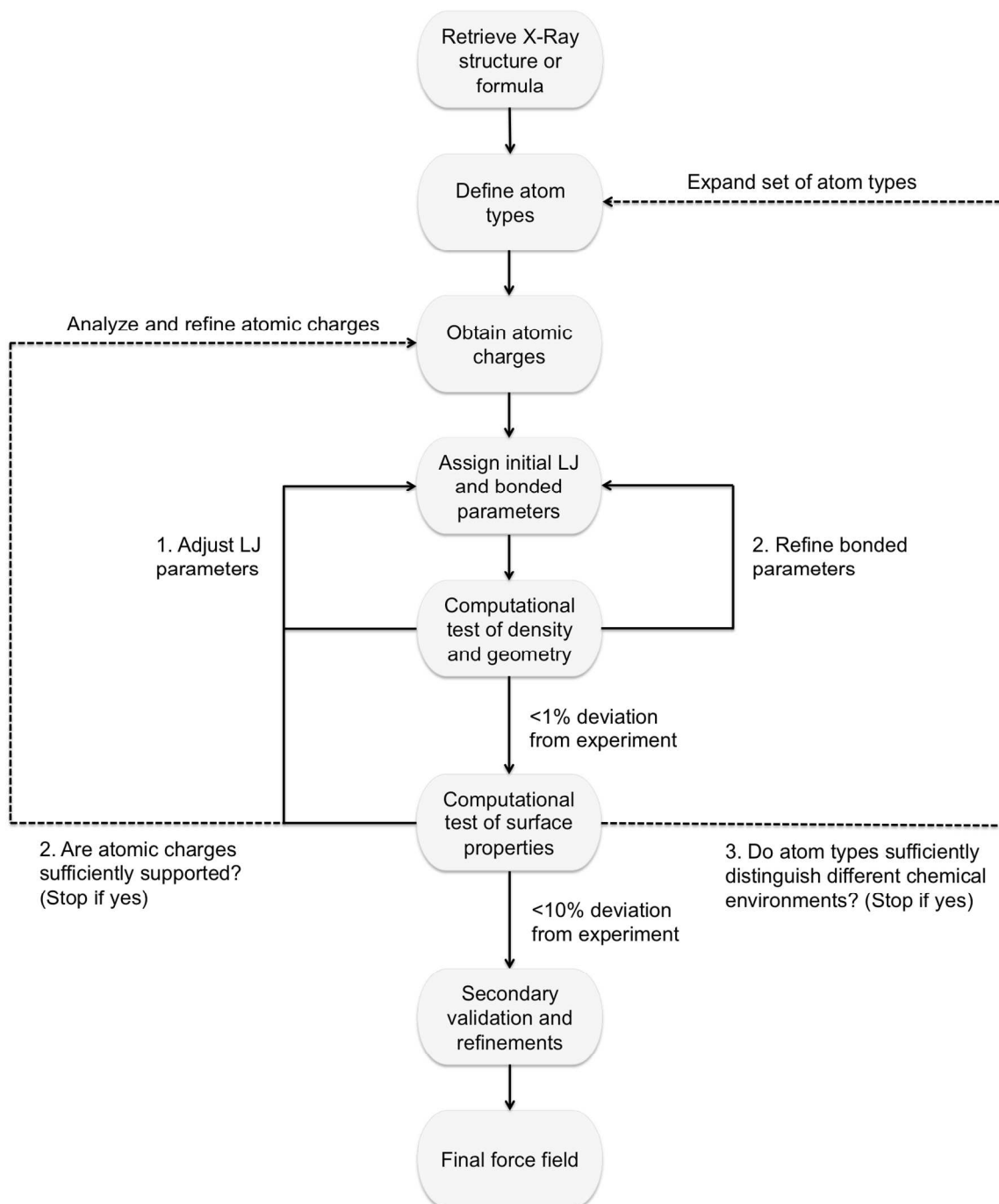


Figure S2. Procedure for parameterization of new and existing compounds in the INTERFACE force field, including the most common refinement loops. Careful assignments in every step in full agreement with physical and chemical understanding minimize the need for loops. In principle, it is possible to go back to any prior step at each stage in the procedure until thermodynamic consistency is achieved. See text in sections 3 and S4.

Table S1. Atomic charges for selected compounds from experimentally measured electron deformation densities and partition into spherical atomic basins using the Hirshfeld method. The values provide a valuable starting point for molecular simulations, especially for polar compounds containing heavy elements. Standard deviations of the last digit are given in brackets (extension of an earlier compilation in ref. 58).

Compound	Atom	Charge in units of e	Reference
LiF	Li	0.95 (3)	S19b
LiI	Li	0.67 (5)	S22b
LiNO ₂ · H ₂ O	Li(H ₂ O)	0.83	S22a
	N	0.51	
	O (nitrite)	-0.67	
NaCl	Na	1.00 (0)	S19b
NaNO ₃ ^a	Na	0.95 (5)	S20b
	N	-0.20 (10)	
	O	-0.25 (10)	
KBr	K	0.8 (1)	S19c
CaF ₂	Ca	2.00 (0)	S19b
MgO	Mg	1.6 (2)	S19a
Al ₂ O ₃	Al	1.32 (5)	S21
AlO(OH)	Al	1.47 (27)	S19d
	H	0.20 (5)	
AlPO ₄ ^b	Al	1.4 (1)	S20a
	P	1.0 (1)	
	CrSO ₄ · 5 H ₂ O ^c	Cr(H ₂ O) ₅	
	S	0.24 (6)	
	O (sulfate)	-0.30 (6)	
Co[O(NC ₅ H ₅)] ₆ (ClO ₄) ₂	Co	1.74 (4)	S24
	Cl	-0.12 (1)	
	O (perchlorate)	-0.15 (4)	
	Pyridine-N-oxide ligand	-0.05 (5) [individual: O -0.83, N 0.27, C ~ -0.2, H ~ 0.3]	
CuSO ₄ · 5 H ₂ O ^c	Cu(H ₂ O) ₅	1.18 (10)	S23
	S	0.06 (2)	
	O (sulphate)	-0.31 (6)	
Cu ₆ Si ₆ O ₁₈ · 6 H ₂ O	Cu	1.23 (6)	S25
	Si	1.17 (15)	
	O (water)	-0.74 (6)	

^a The density of valence electrons near the middle of the N–O bond is high, leading to an uncertainty in atomic charges up to ±0.1e. ^b The crystal structure of AlPO₄ is the same as for tetrahedral SiO₂ (α-quartz) as Al and P are left and right neighbors to Si in the periodic table. The investigation was performed to obtain more information on the charge distribution in the isoelectronic SiO₂, which is noncentrosymmetric, and a Si charge of ~1.2 was inferred. ^c The atomic charges are averaged over different environments. Significant anisotropy was observed, such as charge transfer between the metal cation and coordinated water.

S1. An Overview of Multiscale Simulation Methods

Quantum mechanical methods enable the analysis of the geometry of molecules, conformers, and clusters of molecules including orbitals, transition states, and chemical reactions. The Schrodinger equation only provides an exact solution for one hydrogen atom while larger systems require numerical approximations.^{S27-S29} Computationally affordable and sufficiently realistic solutions of the Schrodinger equation for many electron systems remain an intense area of research.^{10,S30-S33} The best approximation of the electronic structure is obtained using full configuration interaction, which leads to a scaling of computation time with the number of electrons N as $O(N^7)$. Computations beyond small molecules, radicals, and ions are difficult due to the high exponential dependence on system size. Coupled cluster and density functional theory (DFT) methods involve approximations of basis functions, basis sets, and density functionals to reduce the compute expense from $O(N^7)$ to $O(N^3)$ and can be employed to simulate systems up to thousands of atoms. The completion of one picosecond ab-initio MD^{S30} of a peptide in 500 molecules of water using the GGA-PBE functional currently requires approximately 256 processor cores for one week. The convergence in energies using different density functionals, e.g., within the M0x classes, is often not satisfactory.^{10,S31,S34} For example, computed dissociation energies of small molecules from surfaces, cohesive energies of small organic molecules, and electronic excitation energies may differ by a factor up to two. Nevertheless, QM methods are paramount to investigate chemical reactivity and electronic properties at the local scale of chemical bonds, including electron densities, energy levels, conduction, and magnetism. QM methods are less suited to examine properties of systems containing more than several hundred atoms, and limited to time scales of picoseconds. Higher and more compute-expensive

levels of theory are required in particular when heavier elements with d and f electrons are involved.

Access to larger systems is possible using molecular dynamics and Monte Carlo simulations on the basis of a classical Hamiltonian. Compute time scales as $O(N \ln N)$ or $O(N^2)$ with the number of atoms N , depending on the type of summation of pairwise interactions. Folding and self organization of chain molecules in solution and at surfaces in all-atom resolution can be studied as a function of concentration, pH, and ionic strength.^{7,54} Longest recorded simulation times to date exceed milliseconds^{S35} and the completion of 100 nanoseconds classical MD of a protein in 1000 molecules of water with high accuracy of Coulomb interactions currently requires approximately eight processor cores for one week. Access to significant time scales and parallel simulations enables the exploration of complex configuration spaces at length scales of 1 to 1000 nm. Therefore, interfacial assembly, thermal transitions, diffusion, optical switching, and time-dependent mechanical properties can be investigated.^{7,11,51,52,54,65-67,S35,S36} A major limitation is, however, the difficulty to simulate bond dissociation and formation during chemical reactions.

The analysis of structure and dynamics at scales of 10 nm to 1000 μm and nanoseconds to seconds can be achieved using MD and MC simulations on the basis of coarse-grain models. These models involve fewer degrees of freedom compared to atomistic models as every bead represents several, tens, or hundreds of atoms according to the desired level of coarse-graining.^{S37-S39} The energy expression is also simplified, for example, it may contain only bond stretch and van-der-Waals terms.^{S40,S41} When the energy expression and molecular models are chosen interchangeably with a full atomistic description, mapping between full atomistic resolution and coarse grain resolution is possible as well as simulations in dual atomistic/coarse grain resolution. Dissipative Particle Dynamics with soft, interpenetrable particles,^{S42} and field-

based approaches^{S43} can also be employed to access similarly larger length and time scales as with coarse-grain models.

S2. Recent Trends in Interface Simulations

Recent work by many research groups illustrates the variety of problems that can be addressed using simulation techniques at different time and length scales. Current strengths and weaknesses are illustrated by representative examples in this section.

Truhlar et al. have developed state-of-the-art density functionals¹⁰ and utilized the parameters to understand the adsorption of CO and NO molecules on defective MgO {100} and NiO {100} surfaces.^{S31} Chemical bonds to the surfaces can be well characterized yet computed dissociation energies vary by multiples in comparison to experiment. Electronic excitation energies of small molecules have been computed using various density functionals in very good agreement (~10%) with results from higher level methods (MS-CASPT2).^{S32} Ab-initio studies by Goddard et al on gold-carbene complexes explain possible catalytic pathways to form C–C bonds.¹² Knecht and Heinz et al have examined possible catalytic mechanisms of carbon-carbon coupling reactions on peptide-capped Pd nanocrystals using experiment and simulation.⁵⁵ Kremer and Mullen et al. investigated the structure and charge mobility of coronene-type stacked organic semiconductors, using QM methods to derive transfer integrals in combination with measurements.^{S44} van Duin and Goddard et al developed the Reaxx force field to describe chemical reactions of hydrocarbons, silicates, and other compounds.³⁴ Complex bond order terms and highly customized functional terms, however, make it difficult to combine parameters with existing force fields for biopolymers and organic compounds, and reproducible extensions to other compounds are extremely challenging. Ponder et al have developed polarizable force fields for

water and biomolecules (AMOEBA), aiming at better representation of polarity and conformations than all-atom force fields using extensive quantum-mechanical evaluation.³⁸ The energy expression of AMOEBA differs from harmonic force fields such as PCFF, COMPASS, AMBER, CHARMM, GROMACS, and OPLS-AA.

Parker et al calculated the surface energy of spinel using a dedicated Buckingham potential and found an overestimate by more than 50% in comparison to experiment.²⁹ Simulations of hematite and calcite in contact with water showed layering and ion dissolution effects.³⁰ Heinz et al developed a force field for mica-type silicates using common harmonic energy expressions and demonstrated quantitative agreement of computed and measured surface properties.^{11,14} The effectiveness of the approach was later utilized to derive equally dependable parameters for other inorganic compounds that are summarized in the INTERFACE force field.^{7,40,47,48} Self assembly mechanisms of surfactants, thermal transitions, and thermodynamic models for exfoliation in composites have been explained in agreement with available laboratory observations.^{11,49,50,65-67} Cygan et al developed a broader force field for clay minerals which is less accurate in surface properties.^{S10} Cygan and Kirkpatrick et al inspected the mica-water interfacial structure using classical molecular dynamics simulation in good agreement with X-Ray reflectivity data.^{S11} Walsh et al have carried out simulations of DNA binding to titania and peptides binding to quartz surfaces in aqueous solution using classical force fields, aiming at the prediction of the binding mechanism and tailored sequences in comparison to experimental data from phage display.^{45,46} The protonation state of the surfaces, however, was often disregarded. Patwardhan, Heinz, and Perry et al. quantified silica surface compositions in aqueous solution and peptide adsorption mechanisms in agreement with measurements using a thoroughly validated silica force field.⁷ Machesky et al investigated the surface protonation of titania and cassiterite (tin dioxide) using

simulation and experiment,^{S45} and Cummings et al. the adsorption of nucleotides on fullerenes.^{S46}

Heinz et al also proposed a force field for fcc metals⁴⁰ compatible with biomolecular force fields (e.g. CHARMM, AMBER, GROMACS), identified a soft epitaxial adsorption mechanism of peptides on noble metal surfaces in solution⁵² as well as contributions to adsorption by induced charges.⁵¹ Corni et al investigated the interaction of peptide molecules with gold {111} surfaces using ab-initio MD.^{S47} A specialized force field to model adsorption of organic molecules on Au {111} surfaces was derived (GoIP)⁴² and applied to study the interaction of Au {111} surfaces with single amino acids.^{S48} The model requires fixed Au atoms and leads to similar results as CHARMM-METAL.^{S41,40,53} Van der Vegt et al. carried out ab-initio and classical simulations of interactions of amino acids with Ni {111} surfaces^{S49} using a specialized force field that is not transferable to common harmonic energy expressions. Baskes et al developed Embedded Atom Models (EAM) for metals.^{33,S50,S51} The energy expression differs from harmonic force fields for biomolecules and surface energies cannot be quantitatively reproduced unless further fit parameters are included (MEAM). Tight-binding methods for the simulation of metals can be applied at the local scale and possess similar advantages and limitations as DFT methods (section S1).⁶⁸ A review of various simulation approaches to material-biological interfaces was given by Harding et al.^{S52}

Muthukumar et al. have used coarse grain models in combination with experiment to examine the translocation of a polymer through protein pores in a membrane driven by electric fields.^{S53} Another coarse-grain study explains possible packing pathways of a genome in a bacteriophage.^{S54} De Pablo et al derived coarse-grain models of DNA that reproduce trends in salt-dependent melting, bubble formation and rehybridization, as well as approximate

mechanical properties as a function of salt concentration.^{S55} MD simulations of an idealized coarse grain polymer glass under tension and compression helped explain creep behaviour and stress-induced dynamics.^{S56} The directed assembly of block copolymers on nanopatterned and templated surfaces using MC simulation with coarse grain models was investigated,^{S57} and Heinz et al have shown the feasibility of square patterns of block copolymers of small domain spacing in good correlation with experiment.⁶ Kremer et al achieved microsecond simulations of the dynamics of bisphenol A polycarbonate using coarse grain and atomistic models in combination.^{S58} Winfree et al studied the design of nucleic acid sequence and DNA secondary structure using a free-energy based thermodynamic model,^{S59} and applied the concept to the self assembly of DNA tiles into origami patterns.^{S60} Loverde et al investigated the stability of worm-like micelles using dissipative particle dynamics (DPD) with soft coarse grain models and showed details of the budding and break-up mechanism.^{S61}

These and numerous other studies at the length scale of 1 to 1000 nm indicate a variety of different simulation methods and parameter sets that are applied to solve problems related to control interfacial processes.

S3. The Role of Combination Rules for Thermodynamic Consistency

Thermodynamic consistency focuses on the reproduction of key physical, chemical, and surface properties of every compound included in the force field. Once this goal is achieved, combination rules imitate interfacial properties in good quantitative or semi-quantitative precision compared to measurements. Support for the performance of combination rules comes from existing force fields (PCFF, AMBER, CHARMM, GROMACS, OPLS-AA) and from the new parameters for inorganic compounds in the INTERFACE force field. For example,

computed solid-vapor surface tensions and solid-water interfacial tensions of gypsum agree <5% with experiment (Table 1).

The key challenge thus lies in obtaining thermodynamically consistent parameters for a given compound, i.e., the best possible approximation of the electronic structure by available parameters in the classical energy expression. Once achieved, the compound can instantly interact with other compounds in the simulation using standard combination rules. Thereby, each compound maintains the density, surface energy, interface energy, modulus, and other properties in the simulation, and does usually not require specialized interaction potentials with other compounds. More information follows in section S4.5 and limitations are described in section 4.3.

S4. Derivation of Force Field Parameters in Detail

S4.1. Existing Sources and New Developments. Common approaches to the derivation of parameters have been described in the documentation of earlier force fields.^{14,18-28,38,S1,S36,S37,S40} The arguably oldest sources are discussions by Max Born and John Edward Jones on potentials of ionic and molecular solids that are now commonly used as Lennard-Jones potentials.¹⁵⁻¹⁷ While approaches to nonbond parameters vary widely, the derivation of bonded parameters is similar among harmonic force fields.

The parameterization procedure for compounds in the INTERFACE force field involves a sequence of steps that worked well for the parameterization of over thirty different compounds, including inorganic compounds as well as organic molecules and polymers such as PEO (Figures S1 and S2). A key initial step is the definition of chemically equivalent atoms on the basis of the 3D chemical formula and available X-Ray structures. X-Ray structures, tabulated bond lengths

and angles also serve as a guide for values of $r_{0,ij}$ and $\theta_{0,ijk}$ (see equations 1 and 2 in the main text). Tabulated atomic and ionic diameters across the periodic table aid in the assignment of $\sigma_{0,ii}$,^{60,61} and an initial interpretation of the polarizability guides in the assignment of the nonbond well depth $\epsilon_{0,ii}$ for each atom type.⁶⁴ Vibration parameters $k_{rn,ij}$, $k_{\theta n,ijk}$, torsion parameters $V_{\varphi n,ijkl}$, $\varphi_{0n,ijkl}$, atomic charges q_i , and also the Lennard-Jones parameters $\sigma_{0,ii}$ and $\epsilon_{0,ii}$ have often not been associated with a clear physical and chemical rationale in the past. Comparisons of computed properties to readily available experimental data were often missing, parameters relied on quantum-mechanical data without chemical interpretation or analysis of uncertainties, and discrepancies in bulk and surface properties between simulation and experiment up to multiples have been common.^{14,20,21,27,29-33,39-46,S1-S3}

Such uncertainties, however, can be eliminated by clarification of atomic charges q_i ⁵⁸ and by evaluation of computed surface properties of solids in comparison to experiment to assign Lennard-Jones parameters $\sigma_{0,ii}$ and $\epsilon_{0,ii}$.^{14,40} These steps lead to thermodynamic consistency (Table 2 and Figure 3).

S4.2. Atomic Charges. Atomic charges q_i (see equations 1 and 2) approximate the distribution of electron density and quantify the extent of covalent bonding versus ionic bonding (Figure 3).⁵⁸ Atomic charges are experimentally accessible (Table S1) and must be accurately reproduced in the force field. Else, deviations in computed properties arise that cannot be compensated by fitting other parameters without compromising the quality of the force field.^{14,29-31,41,43,45,46,S2,S3,S5,S6-S13} The dependable assignment of atomic charges has been described in ref. 58 and a decade of practice reinforced its key role for reliable simulations.

In short, several methods are suited to deliver appropriate atomic charges and validate their accuracy.⁵⁸ (1) X-Ray deformation densities^{S19-S25} in combination with Hirshfeld partitioning of the measured electron density into spherical atomic basins⁶² yield the best atomic charges for molecular simulations (Table S1). These charges, in combination with van-der-Waals parameters and bonded parameters, typically reproduce dipole moments, cleavage energies, polar contributions to interface tensions, and heats of immersion in agreement with measurements. (2) Similarly, dipole moments yield atomic charges or charges on groups of atoms for many compounds across the periodic table.⁶⁰ The atomic charges from dipole moments are consistent with the charges from X-Ray deformation densities and suitable for molecular simulations. (3) An extended Born model, in association with trends in chemical properties for a set of related compounds across the periodic table, also provides consistent atomic charges, especially if no direct experimental data are available. This method can be as precise as $\pm 0.1e$ and involves a quantitative analysis of covalent and ionic contributions to chemical bonds in a given compound based on available thermochemical data and the coordination environment. Thermochemical data include atomization energies, ionization potentials, and electron affinities, which are readily available for all elements.⁶⁰ The development of density functionals for QM calculations has meanwhile adopted similar practices of referencing thermochemical data.¹⁰ In combination with methods 1 and 2, this approach is fast and accurate for any compound across the periodic table, and entirely based on reported, reproducible chemical insight.⁵⁸ (4) Quantum-mechanical methods must be used with caution (Figure 3a). The derivation of absolute values of atomic charges is not recommended due to possible large deviations.^{58,63,S26} The estimation of relative atomic charges from one compound to another becomes more reliable (i) if the atomic charges

for one compound are exactly known and (ii) if high level basis functions/density functionals are employed.

Atomic charges can be determined within approximately $\pm 5\%$ uncertainty, higher precision is typically not possible related to the anisotropy of the electron density. It is critical, however, to minimize the error, as the sensitivity of interfacial properties, folding of chain molecules, and phase transition temperatures, for example, to the chosen atomic charges is very high in molecular simulations.

Some examples illustrate this sensitivity. (1) Small deviations from appropriate charges in polyethylene oxide at 20 °C (Figure 3a) would lead to phase separation of the polymer in water as opposed to a homogenous solution known from laboratory observations. (2) Atomic charges of Si in tetrahedral O coordination in silicates have been subject to very high uncertainty from +0.5e to +4.0e in various models,^{29-31,41,43,45,46,58,S2,S3,S5,S7-S13} which lead to a spread in computed surface energies up to 100-fold unless the correct value +1.1e ($\pm 0.1e$) is employed.¹⁴ (3) Similar discrepancies are common for Al in octahedral oxygen coordination and many more minerals.⁵⁸ At times, both charges and the surface structure may be misrepresented in models, such as titania surfaces with dangling oxygen bonds in aqueous solution.⁴⁵ (4) Misleading atomic charges using DFT calculations and arbitrary charge partitioning schemes are also reported in other recent parameterizations of silica and silicate hydrates.^{43,46} Associated deviations in interfacial energies then scale with the square of q_i , distort water layering on surfaces, and conformations of adsorbed molecules. Conclusions from simulations using such parameters are questionable and often resonate poorly in the experimental community.⁴³

S4.3. Van-der-Waals Parameters. While the correct polarity ensures an appropriate amount of electrostatic contributions to cohesive energies and interfacial energies, the balance between

Coulomb energies, short-range repulsion, and mid-range attractive van-der-Waals energies is equally important and depends on the parameters $\sigma_{0,ii}$ and $\varepsilon_{0,ii}$ (equations 1 and 2). The nonbond diameter $\sigma_{0,ii}$ reflects the size of the atom or ion and is known across the periodic table.^{60,61} The well depth $\varepsilon_{0,ii}$ reflects the atomic polarizability, expressed via summation of pairwise interactions. Values of $\varepsilon_{0,ii}$ are exactly known for rare gases and Halgren suggested that $\varepsilon_{0,ii}$ increases within a row of the periodic table toward the values for the corresponding rare gas.⁶⁴ In addition, the well depth $\varepsilon_{0,ii}$ depends (i) on the charge state of the atom which changes the polarizability (higher $\varepsilon_{0,ii}$ for negatively charged atoms) and (ii) on the volume density of covalent bonds in the vicinity of the atom, as the cohesion between molecules or surfaces is represented by the values $\varepsilon_{0,ii}$ and by the number of pairwise interactions per unit volume. The latter condition requires smaller $\varepsilon_{0,ii}$ in a dense covalent framework compared to the same atom in small molecules or ions. These factors are not simple to quantify, and therefore a final adjustment of the well depths $\varepsilon_{0,ii}$ to reproduce surface tensions, hydration energies, cleavage energies, and other available surface data is essential (Figure 3b). Equally, a physically consistent interpretation of the values $\varepsilon_{0,ii}$ is important, especially when $\varepsilon_{0,ii}$ values for several atom types need to be determined.

In detail, the interpretation of $\varepsilon_{0,ii}$ involves an initial assessment of $\varepsilon_{0,ii}$ in the context of Halgren's principle within the periodic table, then in the context of the charge state of the atom, and then in the context of the volume density of covalent bonds. Further comparison of suitable $\varepsilon_{0,ii}$ values with $\varepsilon_{0,ii}$ values of the same element in related compounds is highly recommended. As values of $\varepsilon_{0,ii}$ are the most "adjustable" parameters in the force field, it is recommended to check the sensitivity of computed surface properties (e.g. cleavage energy for a solid, cohesive

energy for a liquid) across a range of possible values of $\epsilon_{0,ii}$ (Figure S2). For example, systematic variations of $\epsilon_{0,ii}$ across one order of magnitude for a few slightly different settings of $\sigma_{0,ii}$ each and analysis of a simple computed surface property satisfy this condition. The final assignment of $\epsilon_{0,ii}$ for each atom type i should be accompanied by a full rationale. For a thermodynamically consistent parameterization, it is then often found that a change in $\epsilon_{0,ii}$ by $\pm 5\%$ does not significantly affect the performance of the force field.

Nonbond diameters $\sigma_{0,ii}$ deviate usually $\pm 5\%$ from book value^{60,61} as their interpretation is straightforward. Therefore, their priority in the parameterization is rather low (Table 2) and small adjustments are made to reproduce the experimentally determined density in the simulation. More discussion can be found in ref. 14.

S4.4. Bonded Parameters. Bonded parameters are needed for bond, angle, torsion, and out-of-plane potentials (equations 1 and 2). The assignment of accurate torsion parameters $V_{\varphi n,ijkl}$ and $\varphi_{0n,ijkl}$ is essential to reproduce conformation equilibria of molecules and folding of chain molecules such as proteins in a simulation. Minerals usually require no torsion and no out of plane parameters (equal zero).¹¹ The energy profile during bond rotation, when applicable, involves the superposition of nonbond interactions and bonded interactions. Therefore, the torsion potential serves as an add-on to tune other interactions that are already in place. The derivation of parameters $V_{\varphi n,ijkl}$ and $\varphi_{0n,ijkl}$ for each dihedral angle first requires insight into target values of equilibrium dihedral angles and torsion barriers. These target values are best derived according to (i) experiment (IR, NMR), (ii) stereochemical knowledge and analogies to similar compounds, (iii) quantum-mechanical calculations with appropriate high-level basis sets

or density functionals. The second step is the assignment of parameters in the torsion potential for every dihedral angle to match the energy profile to the chosen target values.

In detail, the assignment of constants $V_{\varphi_{n,ijkl}}$ and $\varphi_{0n,ijkl}$ for each dihedral angle involves (i) an analysis of the torsion profile in the absence of torsion parameters (all $V_{\varphi_{n,ijkl}}$ equal zero), (ii) adjustments in torsion parameters to match the target energy profile, and (iii) testing of the new energy profile using MD simulations of the relevant portion of the chain molecule. To begin, a 5 ns MD simulation of the relevant torsion fragment including first and second bonded neighbors is carried out in vacuum (or in solution, respectively), recording snapshots every 10 fs. A distribution plot of the dihedral angles $A(\varphi)$ is then prepared and converted into a logarithmic plot $E(\varphi) = -RT \ln A(\varphi) + C$ to determine the torsion barriers and equilibrium dihedral angles in the absence of any torsion potential. Then, the barrier heights $V_{\varphi_{n,ijkl}}$ and the angular offsets $\varphi_{0n,ijkl}$ in the trigonometric torsion potential (equations 1 and 2) are edited to match the target values. Finally, the MD simulation is repeated with the new torsion potential to verify the reproduction of target angular minima and energy barriers in the torsion energy profile.

Current torsion potentials for biomolecules such as in CHARMM and AMBER reproduce folding of DNA and proteins up to tens of monomers in length.^{S35,S36} Yet torsion potentials may undergo further possible improvements (1) in the accuracy of torsion barriers and equilibrium angles, (2) specifically in the representation of stereoelectronic effects (e. g. in polyethylene oxide and carbohydrates), (3) and related to the dependence on pH in charged chain molecules. For example, significant differences were found in computed equilibrium angles Φ , Ψ as well as in torsion barriers for short homopeptides (Ser₃, Tyr₃) using different force fields such as CHARMM and CVFF.⁵⁴ Also, the eclipsed rotation barrier of *n*-butane of 3.95 kcal/mol in the gas phase according to IR spectroscopy^{S62} still amounts to 5 to 6 kcal/mol in some force fields

based on older quantum-mechanical results. The higher barrier slows down rotation dynamics in hydrocarbons up to a factor of 30 at room temperature according to the Boltzman factor.

Therefore, the capabilities of force fields to study folding of proteins, DNA, and polyelectrolytes are currently still not fully exploited. Torsion potentials often still rely on partially verified assumptions or “fits” rather than on the interpretation of torsion barriers, as the case of *n*-butane shows. The maximum length of peptides to compute conformations and folding in agreement with experiment is $\sim 10^1$ amino acids in solution. Improved rotation barriers, validated specifically in solution, could enable dependable simulations of folding and self-organization of proteins as long as $\sim 10^2$ amino acids. Examples for the simulation of folding of selected longer chains ($\gg 10$ amino acids) in very good agreement with experiment have been reported,^{S35} however, the results do not imply reliability for other sequences, nor even for the same sequence under different pH, temperature, solvent, and ionic strength using current parameters.

A starting point for the derivation of parameters for bonds ($k_{r,ij}$, $r_{0,ij}$) and angles ($k_{\theta,ijk}$, $\theta_{0,ijk}$) are crystal structures of the mineral, metal, or molecular crystal determined by X-Ray or neutron diffraction, as well as compilations of bond lengths and angles for compounds across the periodic table (Table 2).⁶⁰ Experimentally determined equilibrium bond lengths $r_{0,ij}$ and angles $\theta_{0,ijk}$ can directly be used in the force field. Sometimes minor adjustments due to the additional influence of nonbond interactions become necessary (<5%), for example, when minerals with strong ionic attraction require a slightly higher $r_{0,ij}$ to help offset strong cohesion.

Initial approximations of harmonic force constants $k_{r,ij}$ and $k_{\theta,ijk}$ can be made according to corresponding frequencies in experimental IR and Raman spectra, and by comparison to bonds and angles in similar compounds. Initial parameter choices are then tested by computation of the

IR/Raman spectrum, which involves a short MD simulation (5 ps with recording of coordinates every time step of 1 fs),¹⁴ calculation of the velocity autocorrelation function and Fourier transformation. The force constants are then adjusted until computed vibration frequencies match experiment as closely as possible (see ref. 14 for details). The feasible accuracy in frequencies is usually better than 50 cm^{-1} , while intensities are not reproducible due to neglect of the full electronic structure.

S4.5. Interfaces and Multiphase Materials. For the simulation of interfaces, Lennard-Jones parameters for interactions between different atom types are obtained from parameters for homoatomic interactions (σ_{ij} and ϵ_{ij} from $\sigma_{0,ii}$, $\sigma_{0,jj}$, $\epsilon_{0,ii}$, $\epsilon_{0,jj}$) and reliance on standard combination rules. Thermodynamic consistency for all compounds enables the accurate simulation of mixtures of liquids, solid-liquid interfaces, co-crystals, and multi-component composites. For example, the reliable computation of mineral-water interface tensions is a result of using parameters that yield the surface tension of the solid mineral phase and the surface tension of liquid water in agreement with experiment. Addition of a polyelectrolyte to the solid-liquid interface enables a similarly dependable computation of the adsorption energy, if the parameters of the polyelectrolyte are thermodynamically consistent and reproduce the hydration energy of the polyelectrolyte in agreement with experiment.

It is characteristic that thermodynamically consistent parameters lead to very good agreement of many computed properties with experiment that were not originally fitted. For example, such properties include surface energy anisotropies, surface reconstruction processes, dielectric properties, heat capacity, thermal conductivity, diffusion constants, and elastic constants. Also sensitive properties such as phase transition temperatures (in a range of $\pm 200 \text{ K}$ from the

reference state) and radii of gyration of chain molecules agree well with experiment, such as for the model of polyethylene(oxide) in the INTERFACE force field.

The derivation of force field parameters for organic molecules, solvents, and biopolymers requires the same rigorous assessment as for inorganic compounds. This includes, for example, surface tensions, vaporization energies of liquids at room temperature, short-range molecular orientation (including pi-stacking interactions), and hydration energy.

S4.6. Available Versions of the INTERFACE Force Field and Adaptation to Other Force Field Expressions. All parameters are provided in INTERFACE-PCFF format as part of the Supporting Information. The versions INTERFACE-CHARMM and INTERFACE-CVFF are also available for several compounds. The INTERFACE force field can also be appended to any existing force field based on a harmonic energy expression. Proper interfacing with a different harmonic force field involves all parameters as given in INTERFACE-PCFF (or INTERFACE-CHARMM) format with appropriate adjustments in LJ parameters as described in section 2.2 (no torsion parameters needed for minerals).

The adjustment of LJ parameters (if necessary) first involves a qualitative estimate of the direction and magnitude of changes, guided by known examples for the conversion of LJ parameters from one harmonic force field to another.^{14,40,47,48} Second, a comparison of computed cell parameters to values from experiment (or to values by the original force field) is carried out to test and refine the new LJ parameters until a good fit is achieved. Third, a surface property such as cleavage energy, hydration energy, or cohesive energy is computed using the new force field to probe quantitative equivalence with the original force field (differences in single point energies for two different configurations of the same system may suffice for comparison of original and new force field, rather than obtaining full dynamic data). Usually, a good result is

expected without further adjustments, otherwise the respective part of the original parameterization procedure is followed to optimize the parameters for the new energy expression (sections 3.3. and S4.3., Figures 3b and S2).

Secondary validation of further properties, e.g., mechanical, can also be helpful depending on purpose. The adaptation procedure is straightforward and easier than previous transferability protocols that sometimes also modify atomic charges.

S4.7. Parameterization of New Compounds. Parameters for novel compounds can be obtained using the procedure toward thermodynamically consistent parameters (Figure S2) whereby existing compounds provide helpful benchmarks. The INTERFACE parameterization for a single compound may require a few weeks for experienced users up to several months for less experienced users and consumes 10^3 to 10^4 CPU hours, including the collection of charges and performance of MD simulations to refine parameters until convergence of a variety of properties and agreement with experiment is achieved. Major efforts involve the assignment of atomic charges and often the retrieval of unequivocal experimental reference data (Figure 3).

The procedure also provides parameters for compounds without known experimental or tabulated data in very good approximation. The assignment of initial justified charges and thermodynamically consistent other parameters according to the protocol, in comparison to chemically similar compounds as well as to QM data, provides the best chances for an accurate initial parameterization. For example, cement minerals were initially parameterized in this way, only by help of available X-Ray data and comparison to layered silicates. Retrieval of experimental data for cleavage energies of tricalcium silicate and surface energies of tobermorite from experimental sources at a later time and comparison to computed values required only minor or no adjustments. The same was true for the initial quality of computed mechanical

properties. Ultimately, any parameterization protocol faces the challenge that validation of the force field requires experimental verification of computed predictions and, possibly, iterative improvements.

Secondary validation by computation of a larger array of properties, such as extensive adsorption, mechanical, and thermal data requires additional time. Secondary validation usually confirms expected uncertainties from primary validation and parameter revisions are minor or unnecessary. A consistent interpretation of the parameters for a new compound in the context of existing parameters for similar compounds also allows estimates of uncertainty and reduces the need for extensive secondary validation.

S5. Further Validation and Possible Extensions

S5.1. Reliability of LJ Parameters for FCC Metals. Before ref. 40, LJ parameters for metals were fitted to densities at 298 K and vaporization energies near 3000 K, which leads to poor performance with respect to many properties.^{20,21,27,S4,S6} In ref. 40, we have chosen LJ parameters that reproduce the density at 298 K and the experimentally known surface energy at 298 K, i.e., following thermodynamic consistency, which eliminates many deviations and turns LJ potentials into well-performing models for fcc metals. In addition to densities and surface tensions that are fitted through the choice of $\sigma_{0,ii}$ and $\varepsilon_{0,ii}$, surface energy anisotropies for different facets,⁴⁰ metal-water interface tensions, and the dielectric constant of the first three molecular layers of water adsorbed on gold ($\varepsilon_R = 6, 32, 78$) agree with measurements down from errors by multiples using previous LJ potentials.^{40,51} Also, adsorption energies of peptides and surfactants on even $\{h k l\}$ metal surfaces in solution are consistent with results by phage display and measured adsorption energies.⁵²⁻⁵⁴ Trends in molecule adsorption and specificity to

shaped metal surfaces agree with experimental studies,⁵⁴ and elastic constants in 12-6 potentials agree ~20% with experiment, sometimes even better than 5% as shown for Pd (see Table 1).⁴⁰ Further, the critical size of Pd metal nanoclusters for the transition from amorphous to crystalline at ~1.5 nm is predicted in agreement with TEM and XRD studies.⁵⁵

In particular, a growing number of studies by many research teams provide further evidence for the applicability and accuracy of the models. For example, Petkov et al. found very good agreement between experimentally measured and computed pair correlation functions for Au-Pt alloy nanoparticles of various compositions and insight into local disorder.^{S63} Saiz-Poseu et al. investigated the self-assembly of catechol-based macrocycles on gold {111} surfaces by XPS, STM, and molecular dynamics simulation and identified the influence of solute versus solvent in very good agreement of simulations with measurements.^{S64} Other simulations employed the models to investigate the influence of molecular adsorption on elongating gold nanowires,^{S65} to predict the morphology of self-assembled nanoparticles in diblock copolymers,^{S66} to analyze the structure and dynamics of thiol-functionalized gold nanoparticles in aqueous environment,^{S67} and the possible mechanism of formation of alkanethiol monolayers on gold.^{S68} The parameters for aluminum were also employed in a mesoscale model of electrode interfaces in Li-ion batteries.^{S69} Schatz et al. examined transitions in DNA from A to B form between gold surfaces.^{S70} The parameters for Cu and Au were used in conjunction with DFT calculations to examine interactions of small water clusters with metal surfaces in detail.^{S71,72} Kim et al. used the models in Monte Carlo simulation to explain water meniscus condensation and capillary forces in AFM on gold surfaces.^{S73} Molecular dynamics simulations by Barone et al. provide insight into the self-assembly of tetraphenylporphyrin-based monolayers and bilayers on silver surfaces.^{S74}

S5.2. Layered Silicates. Beyond our own initial studies, the parameters for layered silicates have been used for simulations by various research teams and shown valuable correlations with a broad range of experimental data. For example, Fermeglia, Pricl, and Posocco et al. carried out multiscale simulations of montmorillonite/poly(ethylene oxide) nanocomposites with atomistic detail^{S75} as well as simulations of silylated montmorillonites of different chain length to explain trends in basal plane spacing from X-ray data and the role of silane spacers.^{S76} Cummings et al. carried out simulations of confined liquids between mica layers,^{S77} examined fluid-solid transitions of various confined species,^{S78,S79} and investigated the effect of electric fields on water in mica pores.^{S80} In studies by Pandey et al., the parameters for layered silicates were used to derive coarse grain models for clay minerals and examine the adsorption of peptides.^{S81} Mathew and Luthey-Schulten investigated the influence of the montmorillonite surface on nucleotide oligomerization reactions.^{S82} Jordan et al. showed very good agreement of computed structural properties by the force field in comparison to DFT results.^{S83} Wallis et al. investigated the interlayer structure of montmorillonite containing iron cations and its relation to catalytic activity in oxidative coupling reactions of hydrophobic organic substrates.^{S84} The adsorption of polyaromatic heterocycles on pyrophyllite using the force field and DFT methods was investigated by Sainz-Diaz et al.^{S85} Xu et al. investigated the Young's modulus of effective clay clusters in polymer nanocomposites^{S86} and Berkowitz et al. analyzed restructuring of surfactants on mica surfaces in aqueous solution by molecular dynamics simulation.^{S87}

The procedure to assign atomic charges for various minerals and organic compounds has also been used in many instances by other research teams (not further specified here).^{S8} Although a rigorous algorithmic implementation has not yet been implemented to-date, physical-chemical

principles reported in this procedure (summarized in Figure 3a) are the key to parameter developments in the INTERFACE force field.

S5.3. Comparison with Reactive Potentials and Other Potential Types. As mentioned in section 4.3., the INTERFACE force field cannot describe chemical reactions in its present form, except some special cases such as hydration of plaster of Paris to gypsum, photoisomerization reactions,⁶⁷ the abstraction of metal atoms from the surface of metal nanoparticles in catalytic reactions, or the dissolution of certain ionic species such as alkali, phosphate, and sulfate on surfaces. However, the simplicity of the potential supports extensions to Morse potentials, for example, to model the dissociation of covalent bonds. Such extensions do not fully compromise the use of parameters for biopolymers and organic molecules, as is the case in dedicated reactive force fields. Other possibilities to trace chemical reactions include the combination of the INTERFACE force field with quantum methods on a local scale, the simplified or stepwise simulation of reactions using customized force field parameters for reaction intermediates.

Reactive force fields work well for certain classes of compounds, e.g., ReaxFF is suited for reactions of hydrocarbons³⁴ and AIREBO for carbon compounds.³⁷ A caveat for other compounds is that computed surface properties of reactants or products themselves may deviate considerably from experiment, e.g., surface tensions, hydration energies, or interfaces with water and biomolecules. Moreover, the simulation of interfaces with biopolymers and other phases is difficult due to the lack of parameters in the dedicated format.^{34,37} Therefore, simple customized reactive extensions of the INTERFACE force field based on QM and experimental data for non-reactively parameterized compounds have the potential to yield good results due the focus on accurate properties and few, well defined parameters.

In comparison to embedded atom potentials for metals, the INTERFACE force field is a possible alternative due to the outstanding performance for fcc metals (section S5.2). Further extensions of the INTERFACE parameters may comprise polarizability (for induced charges) and coverage of non-fcc metal structures.

In conclusion, we emphasize that every potential possesses strengths and weaknesses. The INTERFACE force field and harmonic energy expressions are one class among different functional forms of which each provides valuable insight for a certain range of systems and conditions of state.

S6. One-Page Overview of the INTERFACE Force Field

Thermodynamically consistent parameters for inorganic and organic compounds (Table 1) have been integrated in harmonic force fields for organic and biological compounds and compiled as a first version of the INTERFACE force field. The attached INTERFACE-PCFF force field contains parameters added into PCFF (equation 2) as well as molecular models for the following compounds:

- **Layered silicates:** mica, different montmorillonites, pyrophyllite, including surfaces of different CEC and cation distributions according to NMR data
- **Fcc metals:** Ag, Al, Au, Cu, Ni, Pb, Pd, Pt, including {111}, {100}, and {110} surfaces
- **Silica:** bulk minerals as well as surfaces of different degree of ionization for specific pH values and particle sizes
- **Calcium sulfates:** calcium sulfate hemihydrate and gypsum, including different cleavage planes
- **Cement minerals:** tricalcium silicate, tricalcium aluminate, ettringite, monosulfate, tobermorite 11 Å, tobermorite 14 Å, including different cleavage planes
- **Hydroxyapatite:** bulk mineral and different cleavage planes
- **Poly(ethylene oxide):** crystal and polymer chain including gauche effect and approximate solubility (radius of gyration) in water

All models are individually explained in the documentation and ready to use in MD simulations, for example, using Discover, Forcite, and LAMMPS programs. Versions of equivalent force fields, such as INTERFACE-CHARMM, INTERFACE-CVFF, are completed for several compounds.

S7. Additional References

- (S1) (a) Sun, H.; Mumby, S. J.; Maple, J. R.; Hagler, A. T. *J. Am. Chem. Soc.* **1994**, *116*, 2978-2987. (b) Maple, J. R., Thacher, T. S., Dinur, U.; Hagler, A. T. *Chem. Des. Autom. News* **1990**, *5*, 5-10. (c) Sun, H. *J. Comput. Chem.* **1994**, *15*, 752-768. (d) Hill, J.-R.; Sauer, J. *J. Phys. Chem.* **1994**, *98*, 1238 - 1244. (e) Sun, H. *Macromolecules* **1995**, *28*, 701-712.
- (S2) Beest, B. W. H.; Kramer, G. J.; Van Santen, R. A. *Phys. Rev. Lett.* **1990**, *64*, 1955-1958.
- (S3) Collins, D. R.; Catlow, C. R. A. *Am. Mineral.* **1992**, *77*, 1172-1181.
- (S4) Shu, Z.; Davies, G. J. *Phys. Status Solidi A* **1983**, *78*, 595-605.
- (S5) Sanders, M. J.; Leslie, M.; Catlow, C. R. A. *J. Chem. Soc., Chem. Comm.* **1984**, 1271-1273.
- (S6) Uppenbrink, J.; Wales, D. J. *J. Chem. Phys.* **1992**, *96*, 8520-8534.
- (S7) Hill, J. R.; Sauer, J. *J. Phys. Chem.* **1994**, *98*, 1238-1244.
- (S8) Hill, J. R.; Sauer, J. *J. Phys. Chem.* **1995**, *99*, 9536-9550.
- (S9) Teppen, B. J.; Rasmussen, K.; Bertsch, P. M.; Miller, D. M.; Schafer, L. *J. Phys. Chem. B* **1997**, *101*, 1579-1587.
- (S10) Cygan, R. T.; Liang, J. J.; Kalinichev, A. G. *J. Phys. Chem. B* **2004**, *108*, 1255-1266.
- (S11) Wang, J. W.; Kalinichev, A. G.; Kirkpatrick, R. J.; Cygan, R. T. *J. Phys. Chem. B* **2005**, *109*, 15893-15905.
- (S12) Lopes, P. E. M.; Murashov, V.; Tazi, M.; Demchuk, E.; MacKerell, A. D. *J. Phys. Chem. B* **2006**, *110*, 2782-2792.
- (S13) Cruz-Chu, E. R.; Aksimentiev, A.; Schulten, K. *J. Phys. Chem. B* **2006**, *110*, 21497-21508.

- (S14) (a) Brunauer, S.; Kantero, D. L.; Weise, C. H. *Canadian J. Chem.* **1956**, *31*, 729-742. (b) Westwood, A. R. C.; Goldheim, D. L. *J. Appl. Phys.* **1963**, *34*, 3335-3339. (c) Boumiz, A.; Sorrentino, D.; Vernet, C.; Tenoudji, F. C. in *13th Proceedings of the 2nd RILEM Workshop on Hydration and Setting: Why does cement set? An interdisciplinary approach*, Nonat, A., ed.; Dijon, France, 1997.
- (S15) Brunauer, S.; Kantero, D. L.; Weise, C. H. *Canadian J. Chem.* **1959**, *37*, 714-724.
- (S16) (a) Taylor, J. A. G.; Hockey, J. A. *J. Phys. Chem.* **1966**, *70*, 2169-2172. (b) Lamb, R. N.; Furlong, D. N. *J. Chem. Soc., Faraday Trans. 1*, **1982**, *78*, 61-73.
- (S17) (a) Dundon, M. L.; Mack, E., Jr. *J. Am. Chem. Soc.* **1923**, *45*, 2479-2485. (b) Kimura, O. *Bull. Chem. Soc. Jpn* **1942**, *17*, 61-64. (c) Oglesby, M. L.; Gutshall, P. L.; Phillips, J. M. *American Mineralogist* **1976**, *61*, 295-298. (d) Söhnel, O. *J. Crystal Growth* **1982**, *57*, 101-108. (e) Weijnen, M.P.C.; van Rosmalen, G. M.; Bennema, P.; Rijpkema, J. J. M. *J. Crystal Growth* **1987**, *82*, 509-527.
- (S18) The cleavage energy of hydroxyapatite, $\text{Ca}_{10}(\text{PO}_4)_6(\text{OH})_2$ is lower than 1180 mJ/m^2 for $\text{Ca}(\text{OH})_2$, ref. S14a, due to the presence of phosphate ions of lower polarity. The cleavage energy is also higher than 360 mJ/m^2 for $\text{CaSO}_4 \cdot 2 \text{ H}_2\text{O}$, ref. S17a, related to the absence of crystal water and higher polarity of phosphate versus sulfate ions.
- (S19) (a) Brill, R.; Hermann, C.; Peters, C. *Z. Anorg. Allg. Chem.* **1948**, *257*, 151-165. (b) Witte, H.; Wölfel, E. *Rev. Mod. Phys.* **1958**, *30*, 51-55. (c) Aref'ev, K. P.; Vorob'ev, S. A. *Izv. Vuz. Fiz.* **1972**, *15*, 34-38. (d) Hill, R. J. *Phys. Chem. Miner.* **1979**, *5*, 179-200.
- (S20) (a) Thong, N.; Schwarzenbach, D. *Acta Crystallogr., Sect. A* **1979**, *A35*, 658-664. (b) Göttlicher, S.; Knöchel, C. D. *Acta Crystallogr., Sect. B* **1980**, *B36*, 1271-1277.

- (S21) Lewis, J.; Schwarzenbach, D. *Acta Crystallogr., Sect. A: Cryst. Phys., Diffr., Theor., Gen. Crystallogr.* **1982**, *A38*, 733-739.
- (S22) (a) Hermansson, K.; Thomas, J. O. *Acta Crystallogr., Sect. C* **1983**, *C39*, 930-936. (b) Greenwood, N. N.; Earnshaw, A. *Chemistry of the Elements*; Pergamon Press: Oxford, 1984.
- (S23) Vaalstra, T. P.; Maslen, E. N. *Acta Crystallogr., Sect. B* **1987**, *B43*, 448-454.
- (S24) Wood, J. S. *Inorg. Chim. Acta* **1995**, *229*, 407-415.
- (S25) Belokonewa, E. L.; Gubina, Yu. K.; Forsyth, J. B.; Brown, P. J. *J. Phys. Chem. Min.* **2002**, *29*, 430-438.
- (S26) (a) Mulliken, R. S. *J. Chem. Phys.* **1955**, *23*, 1833-1840. (b) Bader, R. F. W. *Chem. Rev.* **1991**, *91*, 893-928.
- (S27) Atkins, P. W.; Friedman, R. S. *Molecular Quantum Mechanics*, 3rd ed.; Oxford University Press: Oxford, 1997.
- (S28) McQuarrie, D. A.; Simon, J. D. *Physical Chemistry – A Molecular Approach*; University Science Books, Sausalito, CA, 1997.
- (S29) *Springer Handbook of Atomic, Molecular, and Optical Physics*, Drake, G. W. F., ed.; Springer, New York, 2006.
- (S30) Krack, M.; Parrinello, M. *Phys. Chem. Chem. Phys.* **2000**, *2*, 2105-2112.
- (S31) Valero, R.; Gomes, J. R. B.; Truhlar, D. G.; Illas, F. *J. Chem. Phys.* **2010**, *132*, 104701.
- (S32) Jacquemin, D.; Perpète, E. A.; Ciofini, I.; Adamo, C.; Valero, R.; Zhao, Y.; Truhlar, D. G. *J. Chem. Theory Comput.* **2010**, *6*, 2071-2085.

- (S33) Westmoreland, P. R.; Kollman, P. A.; Chaka, A. M.; Cummings, P. T.; Morokuma, K.; Neurock, M.; Stechel, E. B.; Vashishta, P. *Applying Molecular and Materials Modeling: An International Comparative Study*; Kluwer Academic, Amsterdam, 2002.
- (S34) Jaguar Program and Graphical Interface. Schrodinger, Inc. 2012.
- (S35) Lindorff-Larsen, K.; Piana, S.; Dror, R. O.; Shaw, D. E. *Science* **2011**, *334*, 517-520.
- (S36) MacKerell, A. D., Jr.; Feig, M.; Brooks, C. L., III *J. Comput. Chem.* **2004**, *25*, 1400-1415.
- (S37) Nath, S. K.; Escobedo, F. A.; de Pablo, J. J. *J. Chem. Phys.* **1998**, *108*, 9905-9911.
- (S38) Harmandaris, V. A.; Adhikari, N. P.; van der Vegt, N. F. A.; Kremer, K. *Macromolecules* **2006**, *39*, 6708-6719.
- (S39) Nielsen, S. O.; Lopez, C. F.; Srinivas, G.; Klein, M. L. *J. Chem. Phys.* **2003**, *119*, 7043-7049.
- (S40) Monticelli, L.; Kandaswamy, S. K.; Periole, X.; Larson, R. G.; Tieleman, D. P.; Marrink, S. J. *J. Chem. Theory Comput.* **2008**, *4*, 819-834.
- (S41) Pandey, R. B.; Heinz, H.; Feng, J.; Farmer, B. L.; Slocik, J. M.; Drummy, L. R.; Naik, R. *Phys. Chem. Chem. Phys.* **2009**, *11*, 1989-2001.
- (S42) Groot, R. D.; Warren, P. B. *J. Chem. Phys.* **1997**, *107*, 4423-4435.
- (S43) Fraaije, J. G. E. M.; vanVlimmeren, B. A. C.; Maurits, N. M.; Postma, M.; Evers, O. A.; Hoffmann, C.; Altevogt, P.; GoldbeckWood, G. *J. Chem. Phys.* **1997**, *106*, 4260-4269.
- (S44) Feng, X. L.; Marcon, V.; Pisula, W.; Hansen, M. R.; Kirkpatrick, J.; Grozema, F.; Andrienko, D.; Kremer, K.; Mullen, K. *Nature Mater.* **2009**, *8*, 421-

- (S45) Machesky, M. L.; Predota, M.; Wesolowski, D. J.; Vlcek, L.; Cummings, P. T.; Rosenqvist, J.; Ridley, M. K.; Kubicki, J. D.; Bandura, A. V.; Kumar, N.; Sofo, J. O. *Langmuir* **2008**, *24*, 12331-12339.
- (S46) Zhao, X. C.; Striolo, A.; Cummings, P. T. *Biophysical J.* **2005**, *89*, 3856-3862.
- (S47) Calzolari, A.; Cicero, G.; Cavazzoni, C.; Di Felice, R.; Catellani, A.; Corni, S. *J. Am. Chem. Soc.* **2010**, *132*, 4790-4795.
- (S48) Hoefling, M.; Iori, F.; Corni, S.; Gottschalk, K. E. *Langmuir* **2010**, *26*, 8347-8351.
- (S49) Schravendijk, P.; Ghiringhelli, L. M.; Delle Site, L.; van der Vegt, N. F. A. *J. Phys. Chem. C* **2007**, *111*, 2631-2642.
- (S50) Baskes, M. I.; Melius, C. F. *Phys. Rev. B* **1979**, *20*, 3197-3204.
- (S51) Baskes, M. I. *Phys. Rev. Lett.* **1999**, *83*, 2592-2595.
- (S52) Harding, J. H.; Duffy, D. M.; Sushko, M. L.; Rodger, P. M.; Quigley, D.; Elliott, J. A. *Chem. Rev.* **2008**, *108*, 4823-4854.
- (S53) Wong, C. T. A.; Muthukumar, M. *J. Chem. Phys.* **2010**, *133*, 045101.
- (S54) Forrey, C.; Muthukumar, M. *Biophysical J.* **2006**, *91*, 25-41.
- (S55) Knotts, T. A.; Rathore, N.; Schwartz, D. C.; de Pablo, J. J. *J. Chem. Phys.* **2007**, *126*, 084901.
- (S56) Riggleman, R. A.; Schweizer, K. S.; de Pablo, J. J. *Macromolecules* **2008**, *41*, 4969-4977.
- (S57) Detcheverry, F. A.; Liu, G. L.; Nealey, P. F.; de Pablo, J. J. *Macromolecules* **2010**, *43*, 3446-3454.
- (S58) Hess, B.; Leon, S.; van der Vegt, N.; Kremer, K. *Soft Matter* **2006**, *2*, 409-414.
- (S59) Dirks, R. M.; Lin, M.; Winfree, E.; Pierce, N. A. *Nucl. Acids Res.* **2004**, *32*, 1392-1403.

- (S60) Fujibayashi, K.; Hariadi, R.; Park, S. H.; Winfree, E.; Murata, S. *Nano Lett.* **2008**, *8*, 1791-1797.
- (S61) Loverde, S. M.; Ortiz, V.; Kamien, R. D.; Klein, M. L.; Discher, D. E. *Soft Matter* **2010**, *6*, 1419-1425.
- (S62) Herrebout, W. A.; van der Veken, B. J.; Wang, A.; Durig, J. R. *J. Phys. Chem.* **1995**, *99*, 578-585.
- (S63) Petkov, V.; Wanjala, B. N.; Loukrakpam, R.; Luo, J.; Yang, L.; Zhong, C. J.; Shastri, S. *Nano Letters* **2012**, *123*, 4289-4299.
- (S64) Saiz-Poseu, J.; Martinez-Otero, A.; Roussel, T.; Hui, J. K. H.; Montero, M. L.; Urcuyo, R.; MacLachlan, M. J.; Farauto, J.; Ruiz-Molina, D. *Phys. Chem. Chem. Phys.* **2012**, *14*, 11937-11943.
- (S65) French, W. R.; Iacovella, C. R.; Cummings, P. T. *J. Phys. Chem. C* **2011**, *115*, 18422-18433.
- (S66) Posocco, P.; Posel, Z.; Fermeglia, M.; Lisal, M.; Pricl, S. *J. Mater. Chem.* **2010**, *20*, 10511-10520.
- (S67) Heikkila, E.; Gurtovenko, A. A.; Martinez-Seara, H.; Hakkinen, H.; Vattulainen, I.; Akola, J. *J. Phys. Chem. C* **2012**, *116*, 9805-9815.
- (S68) Ahn, Y.; Saha, J. K.; Schatz, G. C.; Jang, J. K. *J. Phys. Chem. C* **2011**, *115*, 10668-10674.
- (S69) Awarke, A.; Wittler, M.; Pischinger, S.; Bockstette, J. *J. Electrochem. Soc.* **2012**, *159*, A798-A808.
- (S70) Lee, O. S.; Cho, V. Y.; Schatz, G. C. *J. Phys. Chem. C* **2012**, *116*, 7000-7005.
- (S71) Nadler, R.; Sanz, J. F. *J. Mol. Model.* **2012**, *18*, 2433-2442.

- (S72) Nadler, R.; Sanz, J. F. *J. Chem. Phys.* **2012**, *137*, 114709.
- (S73) Kim, H. J.; Smit, B.; Jang, J. K. *J. Phys. Chem. C* **2012**, *116*, 21923-32931.
- (S74) Barone, V.; Casarin, M.; Forrer, D.; Monti, S.; Prampolini, G. *J. Phys. Chem. C* **2011**, *115*, 18434-18444.
- (S75) Toth, R.; Voorn, D. J.; Handgraaf, J. W.; Fraaije, J. G. E. M.; Fermeglia, M.; Pricl, S.; Posocco, P. *Macromolecules* **2009**, *42*, 8260-8270.
- (S76) Piscitelli, F.; Posocco, P.; Toth, R.; Fermeglia, M.; Pricl, S.; Mensitieri, G.; Lavorgna, M. *J. Colloid Interface Sci.* **2010**, *351*, 108-115.
- (S77) Cummings, P. T.; Docherty, H.; Iacovella, C. R.; Singh, J. K. *AIChE Journal* **2010**, *56*, 842-848.
- (S78) Docherty, H.; Cummings, P. T. *Soft Matter* **2010**, *6*, 1640-1643.
- (S79) Srivastava, R.; Docherty, H.; Singh, J. K.; Cummings, P. T. *J. Phys. Chem. C* **2011**, *115*, 12448-12457.
- (S80) Srivastava, R.; Singh, J. K.; Cummings, P. T. *J. Phys. Chem. C* **2012**, *116*, 17594-17603.
- (S81) Drummy, L. F.; Jones, S. E.; Pandey, R. B.; Farmer, B. L.; Vaia, R. A.; Naik, R. R. *ACS Appl. Mater. Interf.* **2010**, *2*, 1492-1498.
- (S82) Mathew, D. C.; Luthey-Schulten, Z. *Orig. Life Evol. Biosph.* **2010**, *40*, 303-317.
- (S83) Voora, V. K.; Saidi, W. A.; Jordan, K. D. *J. Phys. Chem. A* **2011**, *115*, 9695-9703.
- (S84) Wallis, P. J.; Chaffee, A. L.; Gates, W. P.; Patti, A. F.; Scott, J. L. *Langmuir* **2010**, *26*, 4258-4265.
- (S85) Sainz-Diaz, C. I.; Francisco-Marquez, M.; Vivier-Bunge, A. *Environmental Chemistry* **2011**, *8*, 429-440.
- (S86) Xu, W.; Zeng, Q. H.; Yu, A. B. *Polymer* **2012**, *53*, 3735-3740.

(S87) Das, J.; Eun, C. S.; Perkin, S.; Berkowitz, M. L. *Langmuir* **2011**, *27*, 11737-11741.